Journal of Membrane Science & Research

journal homepage: www.msrjournal.com

Research Paper

Unlocking the Potential of Networked Cellulose for the Enhanced Nanofiltration Performance of TFC Membranes

Shabin Mohammed, Jamaliah Aburabie, Raed Hashaikeh *

NYUAD Water Research Center, Department of Engineering, New York University Abu Dhabi, Abu Dhabi P.O. Box 129188, United Arab Emirates

Article info

Received 2024-03-23
Revised 2024-04-02
Accepted 2024-04-02
Available online 2024-04-02

Keywords

TFC
Wrinkled membrane
Polyamide
Networked cellulose
Nanofiltration
Cellulose fiber

Highlights

- Investigated the potential of Networked Cellulose (NC) derived from sustainable and cheap resources as a filler for thin film composite membranes
- The presence of NC improved hydrophilicity and rendered wrinkled morphology to the polyamide layer providing enhanced permeability
- At optimum conditions, membranes modified with NC exhibited a pure water permeance of 19.12 ± 1.7 $Lm^{-2}h^{-1}bar^{-1}$ which is 165% higher than pristine membranes

Graphical abstract

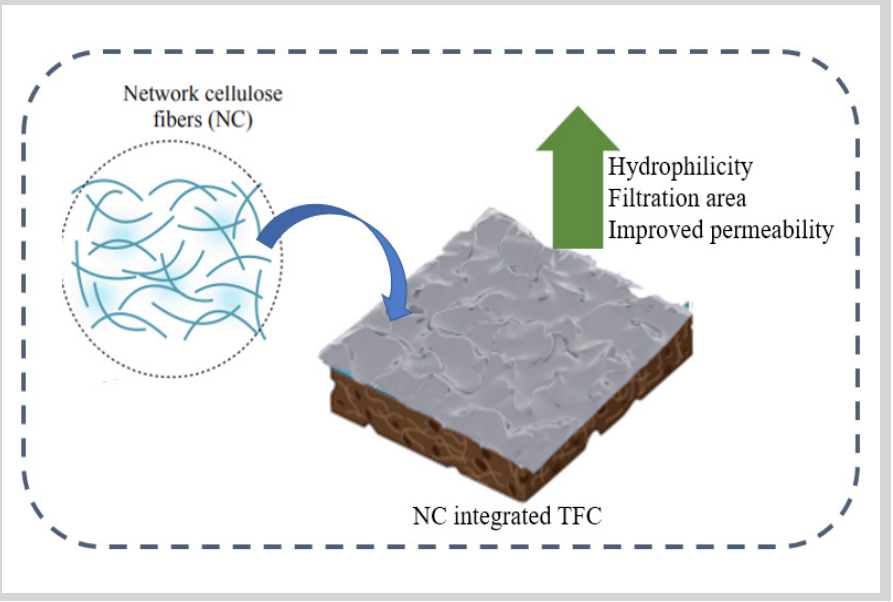

Abstract

Thin-film composite (TFC) membranes have been widely employed for desalination and water treatment to achieve superior separation performance. TFC membranes having a thin active polyamide (PA) selective layer supported by a highly porous support layer have been demonstrated to provide enhanced permeability maintaining excellent salt rejection. Several modifications have been introduced in the TFC layers to advance their membrane performance further. This study proposes incorporating networked cellulose (NC) in the aqueous layer leading to a wrinkled polyamide selective layer with improved filtration area and hydrophilicity rendering significantly enhanced membrane permeance. The less explored NC with highly networked interconnected cellulose fibers was incorporated into the separation layer by simply dispersing in the Piperazine (PIP) solution followed by interfacial polymerization with 1,3,5-Benzenetricarbonyl trichloride (TMC). The TFC membrane with optimum NC loading provided a pure water permeance of 19.12 ± 1.7 $Lm^{-2}h^{-1}bar^{-1}$ (remarkably higher than pristine TFC with 7.2 ± 0.46 $Lm^{-2}h^{-1}bar^{-1}$) while maintaining $MgSO_4$ and Na_2SO_4 rejection above 90%. This study successfully demonstrated the potential use of NC as a low-cost and nontoxic filler to improve the performance of polyamide nanofiltration membranes for water desalination.

1. Introduction

The shortage of adequate and safe water continues to be one of the most urgent issues of our time, worsened by rising population, fast industrialization, and rapidly changing climatic conditions [1]. In addition to this, environmental degradation and strict water quality regulations in place necessitate the need for the development of novel water treatment technologies [2]. Sea water desalination and wastewater treatment through membrane-based technologies is considered a promising strategy to cope with the increasing demand for freshwater [3]. In particular, nanofiltration (NF) requiring lower operating

* Corresponding author: raed.hashaikeh@nyu.edu (R. Hashaikeh)

DOI: 10.22079/JMSR.2024.2025269.1657

pressure and compact structure is highly energy efficient for the removal of contaminants from wastewater, recovering valuable minerals from brine, or as pre-treatment to seawater desalination through reverse osmosis [4, 5]. Extensive research has been devoted to developing novel nanofiltration membranes using various polymeric, ceramic, and other inorganic materials targeting superior separation performance [6, 7]. To date, polymeric membranes are the most attractive considering their scalability and low production cost [8]. A dense cross-linked polymer structure can offer molecular-level separation which is favorable for nanofiltration applications.

For achieving superior membrane performance, NF membranes are conventionally fabricated with a thin film composite (TFC) structure, where a thin separation layer is backed with a highly porous macro-porous support [9]. Different from symmetric membranes characterized by a thicker separation layer across the entire membrane thickness, TFC membranes possess an ultra-thin selective layer providing lower transport resistance. The selective layer is often made of a polyamide network which is responsible for the membrane selectivity while the microporous support provides sufficient mechanical strength without affecting the membrane permeability [10]. Fabrication of such an ultrathin PA layer is achieved through a spontaneous interfacial polymerization reaction between an aqueous amine phase and an organic phase consisting of a monomer with an acyl chloride functional group [11]. While the permeance offered by commercially available polyamide NF membranes is limited to 10 $Lm^{-2}h^{-1}bar^{-1}$, extensive research has been carried out in recent years to improve the overall membrane performance by altering the different fabrication conditions. A thinner selective layer significantly increases the permeance, but this would be highly challenging in terms of scalability considering the difficulties in achieving a defect-free selective layer [12]. As an alternative, the addition of nanofillers in the support layer, intermediate or selective layer has been demonstrated as an effective strategy to enhance the overall performance of TFC membranes [13-16]. However, altering the support layer has limited influence on the overall membrane performance as it is well established that the permselectivity of such membranes is mostly governed by the polyamide selective layer. On the other hand, as the intermediate layer is typically not joined by a chemical bond, adding an intermediate layer could result in instabilities when operated over a longer period of time due to the low adhesion of the polyamide layer to the support [17]. Meanwhile, the addition of fillers in the selective layer improves the hydrophilicity, surface roughness, and surface charge density of TFC membranes eventually resulting in increased water permeability, salt rejection, and chlorine resistance of the membrane [16]. In view of this, non-toxic fillers and membrane materials derived from sustainable and renewable sources are getting increasingly popular as additives in membrane fabrication, considering their cheap availability and environmental friendliness [18-20].

Cellulose and its derivatives are frequently utilized in membrane fabrication owing to its abundant availability, chemical stability, biodegradability, and biocompatibility [21, 22]. As a member of the cellulose nanomaterial family, networked cellulose (NC) is a green and non-toxic material produced from renewable and sustainable resources [23]. NC produced by processing native cellulose by controlled dissolution in sulfuric acid and regeneration, possesses a highly networked structure with excellent structural stability and hydrophilicity. The utilization of cellulose-based materials specifically for polyamide TFC membranes has been demonstrated by few researchers in the past owing to its favorable properties derived from the abundant functional groups [24-28]. The presence of hydroxyl groups not only imparts strong hydrophilic properties but also ensures excellent compatibility in the polymer matrix due to its reaction with the acyl chloride group to form ester bonds during interfacial polymerization [28]. Furthermore, the unique networked structure of cellulose fibers in NC provides possibilities for achieving morphological variations in the selective layer which is anticipated to enhance the overall membrane permeability [29]. Therefore, this study aims to investigate the potential of incorporation of NC in the selective layer to advance the nanofiltration performance of polyamide-based TFC membranes. Integration of NC within the selective layer was achieved by adding various concentrations of NC in the amine solution before interfacial polymerization. The variations in membrane properties and corresponding changes in membrane performance with NC loading have been carefully investigated. Our findings demonstrated that the permeability of TFC membranes could be considerably enhanced by the mere integration of NC in the polyamide layer leading to variations in the morphology and hydrophilicity.

2. Methods

2.1 Materials

PSf pellets (average Mw ~35000 g mol^{-1}), Polyvinylpyrrolidone (PVP) powder (Mw ~55000 g mol^{-1}), n-Methyl-2-Pyrrolidone (NMP), Piperazine (PIP) (99%), 1,3,5-Benzenetricarbonyl chloride (TMC), H_2O_2 (30%), dialysis bag (MWCO 14000 Da), Sodium Chloride (NaCl), Magnesium Chloride ($MgCl_2$), Magnesium Sulfate ($MgSO_4$) and Sodium Sulfate (Na_2SO_4) and Ethanol were purchased from Sigma-Aldrich. Microcrystalline cellulose (MCC) powder and Sulfuric acid (H_2SO_4) Reagent Grade (95–97%) were purchased respectively from FMC BioPolymer (AvicelPH101) and VWR Chemicals USA. Without any additional purifications, all chemicals were utilized just as supplied. Milli-Q water was used to create aqueous monomer and salt solutions.

2.2. Preparation of NC suspension

NC was prepared by acid dissolution and subsequent regeneration following a protocol developed in our group previously [30]. Initially, 10 g of MCC powder was mixed with 100 mL of H_2SO_4 to perform acid hydrolysis using a Copley Dissolution Tester (DIS 6000)-UK. The suspension was stirred for an hour at 200 rpm controlling the temperature at 5 ºC using ice packs. As a result of the acid hydrolysis, the resulting solution looked thick and transparent. The regeneration of cellulose networked structures was then accomplished by the addition of ethanol as a regeneration solvent, which was kept at 5 ºC. To guarantee full regeneration of cellulose fibers, the solution was stirred for an additional twenty minutes. After centrifugation and dialysis to remove the acid, the resulting solution was further filtered, and a mechanical homogenizer (IKA-T25 ULTRA-TURRAX) was used to disperse the fibers uniformly. To isolate finer NC structures, the final NC suspension in water was centrifuged again at 2000 rpm, and the supernatant was utilized to fabricate membranes similar to our previous study [31].

2.3. Fabrication of TFC PA membranes

Fabrication of membrane support: Using non-solvent-induced phase inversion, PSf membrane supports were first fabricated in accordance with our earlier study [32]. To obtain a homogenous polymer casting solution, 17% PSf and 3% PVP were first dissolved in NMP and stirred overnight at 60°C. After allowing the solution to reach room temperature, a semi-automatic casting machine (PMI Porous Materials Inc. Model BT FS- TC, US) was used to cast it on a glass plate at a casting thickness of 200 µm and a constant shear rate of 200 s^{-1}. After holding for 10s, the glass plate containing the polymer film was submerged in a DI water bath to induce phase inversion. As prepared membrane supports were finally stored in DI water for three days, changing the water bath every twelve hours to minimize the impact of any residual NMP and PVP.

Fabrication of selective layer: Formation of the polyamide selective layer was carried by interfacial polymerization with the help of a plate and frame holder (Fig. S1), which held the wet membrane supports with the denser surface exposed to air. To fabricate pristine TFC membranes, the membrane support was initially exposed to an aqueous solution containing PIP monomers (2%) for 5 mins. After removing excess PIP solution from the surface using a gentle air gun and filter paper, interfacial polymerization was carried out by reacting with TMC solution in hexane (0.35%) for a short period of 20 s. The membrane formed was finally cleaned with pure hexane to remove unreacted TMC and subsequently dried in the oven for 60℃ for 3 mins before storing it in Milli-Q water. The preparation of TFC membranes incorporating NC has been done in a similar fashion except that NC at the desired concentration has been added initially to the amine solution with the help of sonication. Membranes were labeled as PA-0, PA-0.0025, PA-0.005, PA-0.01, and PA-0.015 depending upon the amount of NC added in the PIP solution used for membrane fabrication as summarized in Table 1.

Fig. 1 schematically illustrates the steps involved in the fabrication of selective layer preparation.

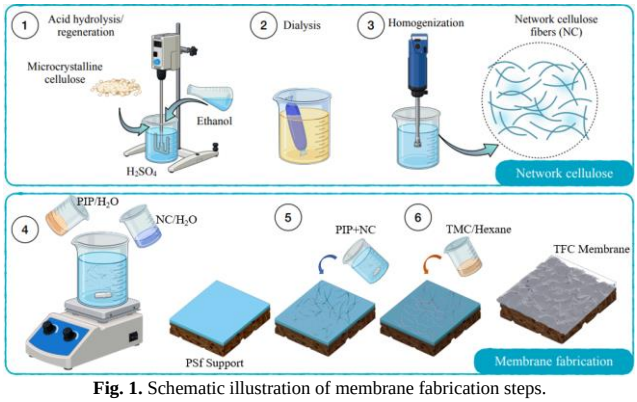

Fig. 1. Schematic illustration of membrane fabrication steps.

Table 1
The concentration of NC in the aqueous phase for different TFC membranes.

Membrane	The concentration of NC in the aqueous phase (%)
PA-0	0
PA-0.0025	0.0025
PA-0.005	0.005
PA-0.01	0.01
PA-0.015	0.015

2.4. Characterization

The morphology, crystal structure, and chemical functional groups of the NC were initially characterized through Transmission Electron Microscopy (TEM), X-ray diffraction (XRD) analysis, and Fourier Transform Infrared (FTIR) spectroscopy. For TEM imaging, the sample was prepared by placing a drop of dilute NC dispersion on agar scientific® holey carbon S147-4 grids and allowing it to dry at ambient conditions. Crystal changes during the formation of NC were investigated by capturing diffraction patterns in the 2θ range of 5−40° at room temperature using X-ray Powder Diffraction (Malvern™, Empyrean 2, Malvern, UK) at a scan rate of 2° min^{-1}. To characterize the functional groups on the NC sample, Fourier transform infrared (FTIR) spectra were recorded in a range of 500 cm^{-1} to 4000 cm^{-1} using a spectrometer (Thermo ScientificTM, Nicolet iS5 with iD7 ATR attachment) by 64 scans at a resolution of 4 cm^{-1}.

Before characterization, all membranes were allowed to air dry. SEM imaging was carried out using FEI Quanta 450 FEG operating at an accelerating voltage of 10 kV to examine the membrane's surface and cross-section. Before imaging, samples were coated with gold to avoid sample charging. Changes in the chemical functional groups on the membrane surface were similarly investigated through FTIR analysis explained previously. The sessile drop method (DSA100, Krüss GmbH, Hamburg, Germany) was utilized to measure the water contact angle (WCA) to assess the hydrophilicity of the membrane. To assure the accuracy of the results, an average value from five distinct locations on the same membrane is presented.

2.5. Evaluation of nanofiltration performance

To assess the nanofiltration performance, the membrane permeance and rejection towards different salt solutions were evaluated using a bench-top stainless-steel dead-end filtration setup (Sterlitech USA). A schematic diagram of the dead-end filtration unit that is utilized in all filtration studies is presented in Fig. S2. Membranes were cut into circular samples with a 2.5 cm diameter reducing the effective surface area to 3.14 cm^2. For the nanofiltration experiments, a pressure difference of 6 bar was employed across the membrane. Aqueous solutions (1000 ppm) of NaCl, $MgCl_2$, Na_2SO_4, and $MgSO_4$ were used to evaluate separation performance. All experiments were carried out with constant magnetic stirring to reduce concentration polarization. The concentrations of the feed and permeate solutions were examined by conductivity measurements. The permeance and rejection values presented here are the average of at least three independent tests in order to ensure the validity of the findings. Rejection and permeance were calculated using the following formula.

$$Permeance = \frac{V}{A.\Delta t.\Delta P} \quad (1)$$

where V is the volume of permeate, Δt is the time required, A is the membrane effective testing area and ΔP is the transmembrane pressure.

$$Rejection = 1 - \frac{C_P}{C_f} \quad (2)$$

where C_p and C_f are the concentration of permeate and feed, respectively.

3. Results & Discussion

3.1. Characterization of NC

Morphological features of the NC fibers can be seen in the TEM images presented in Fig. 2a. As seen in the images, NC is composed of network structures of cellulose II with fibers having varying thicknesses. As reported previously, during hydrolysis and regeneration, the cellulose chain randomly splits, entangles, and bundles together to create a networked form [30]. During the regeneration process, the chains randomly bond to one another and precipitate as a result of solvent exchange. However, rapid precipitation resulted in shorter lengths. To obtain finer networked structures, NC suspension which originally with a mean size of 959 nm was refined with the help of a centrifuge resulting in a final dispersion with an average particle size of 397.7 nm as per DLS measurements (Fig. S3 and S4). FTIR spectra presented in Fig. 2b compare the chemical groups on the NC chains and with the precursor MCC. Both samples exhibited identical peaks indicating no significant changes in the functional groups and the absence of any residual acids or contaminants in the NC. Prominent peaks included those corresponding to OH, C-H, C-O-H, and C-O-C represented by the absorption peaks at about 3000-3500 cm^{-1}, 2890 cm^{-1}, and 1040 cm^{-1}, respectively [33, 34]. Similarly, the XRD pattern obtained for the freeze-dried NC is compared with MCC which is displayed in Fig. 2c. While MCC is characterized by its distinctive crystalline cellulose I peak, NC displayed a less-ordered, amorphous cellulose pattern with characteristics of cellulose II [35]. This indicates that the acid hydrolysis has significantly affected the crystallinity of the material. As the ability of cellulose to absorb water is greatly enhanced in its amorphous phase, the decrease in crystallinity will be favorable for enhancing membrane hydrophilicity [36].

3.2. Membrane characterization

The differences in the chemical functional groups on the various membranes with the PES support are investigated using the FTIR spectra presented in Fig. 3. The spectra show that all samples exhibited peaks from the PSf support, which comprised methyl groups at 2968 cm^{-1}, ether bonds at 1240 cm^{-1}, and aromatic rings at 1490 and 1585 cm^{-1} [32, 37]. In addition to these peaks from the functional groups on PSf, TFC membranes showed peaks around 1442 and 1660 cm^{-1} confirming the formation of a polyamide layer through interfacial polymerization reaction [32, 38]. These peaks correspond to the stretching vibration of C=O of the amide groups. Moreover, TFC membranes also displayed a broad peak around 3410 cm^{-1} which could be assigned to the residual hydroxyl groups from the TMC. Due to the low amount of NC in the membrane, no significant peaks corresponding to NC were observed even for PA-0.015 fabricated with the highest NC content.

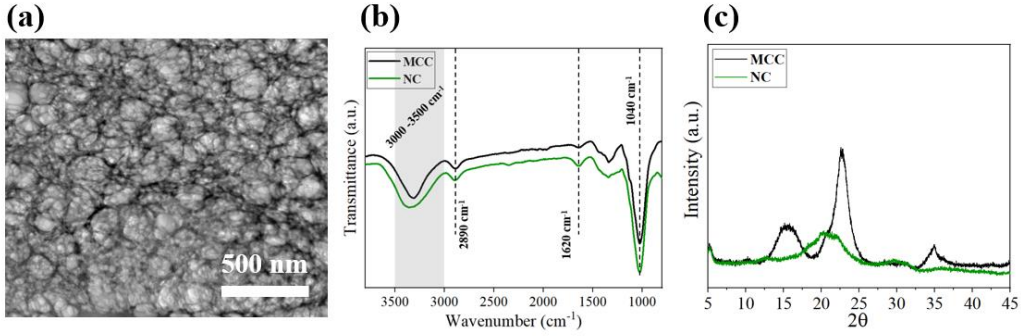

Fig. 2. Characterization of NC. (a) SEM image, (b) comparison of FTIR, and (c) XRD of NC with MCC.

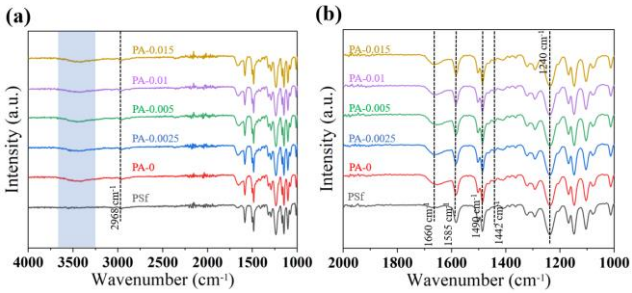

Fig. 3. Comparison of FTIR peaks of different TFC membranes with the PSf support.

SEM images were captured to investigate the surface morphological features of all fabricated membranes and are presented in Fig. 4. As seen in Fig. 4a, the pristine membranes exhibited a relatively smoother dense polyamide selective layer comprising of the typical nodular structure formed by the interfacial polymerization reaction [39]. Besides this, no specific morphological features were observed for pristine TFC membranes. However, adding NC to the monomer solution significantly impacted the polyamide formation, resulting in several randomly aligned wrinkled structures. Consequently, all composite membranes comprising NC resulted in wrinkles directly associated with the amount of incorporated concentration of NC in the monomer solution. Therefore, membranes fabricated with relatively larger amounts of NC exhibited larger areas with interconnected wrinkled structures which is highly recommended for enhancing the membrane permeance [40]. It is widely established that the distribution of amine monomer and its migration towards the organic phase, which results in an IP reaction, have a significant impact on the shape of the PA layer. As evident from the SEM images, the highly wrinkled morphology displayed by the composite membranes could be attributed to the presence of NC that not only provided a rugged reaction interface but also created interfacial instabilities. For instance, the shape of the formed PA layer often resembles the initial water layer containing the amine monomer as the polymerization reaction happens instantaneously at the aqueous/organic interface [41]. As a result, the presence of hydrophilic NC in the aqueous monomer solution provides a rough reaction interface rendering a crumpled morphology. Moreover, although the hydrophilic characteristics of NC favor better absorption of amine monomers, this will also limit the diffusion of PIP molecules into the organic phase [38]. Consequently, it will lead to a non-uniform distribution of monomers and controlled diffusion providing diffusion-driven interfacial instabilities leading to a wrinkled morphology [42]. It is also worth noting that the pristine TFC membranes were characterized by larger nodular structures relative to the composite membranes as evident from the surface SEM images. The presence of hydrophilic NC has facilitated the controlled release of amine monomers leading to a smoother and thinner polyamide layer with smaller nodular features as reported previously [43]. Cross-sectional images presented further confirm the thinning of the selective layer upon higher NC presence in the aqueous phase. For instance, the selective layer thickness which was originally around 295 nm for pristine polyamide membrane gradually decreased to 211 nm for the case of PA-0.015.

The surface morphology was further analyzed through AFM to investigate the influence of the formed wrinkles on the effective membrane filtration area. The captured images are presented in Fig. 4 and the comparison of surface area and roughness parameters are respectively displayed in Fig. 5a and b. It is worth noting that, the roughness parameters proportionally increased with the addition of NC in the fabrication solution. A higher surface roughness is often accompanied by an increase in the effective surface area available for transport [44]. To investigate this, variations in surface area have been studied by comparing the percentage increase in AFM-measured surface area with the projected surface area for various membranes. The projected area of 400 μm^2 has been fixed for all the membranes and has been used to measure the effective surface area available for filtration using AFM software. As seen in Fig. 5a, the change in surface area proportionally increased with the addition of NC in the fabrication solution. For example, while pristine PA-0 showed a 1.22% increase in surface area, PA-0.0025, PA-0.005, PA-0.01, and PA-0.015 displayed an increase of 3.1, 5.32, 9.87, and 10.58% respectively. An increase in surface area for the pristine membrane is due to the nodular morphology of the polyamide layer, while the subsequent gradual increase in the surface area could be attributed to the wrinkled morphology induced by the underlying NC. Nevertheless, PA-0.015 displayed a similar enhancement in the surface area to that of PA-0.01 despite the increased presence of NC. This could be due to the increased smoothness of the localized areas within the proximity of NC that formed considerably smaller nodular structures within the selective layer [38].

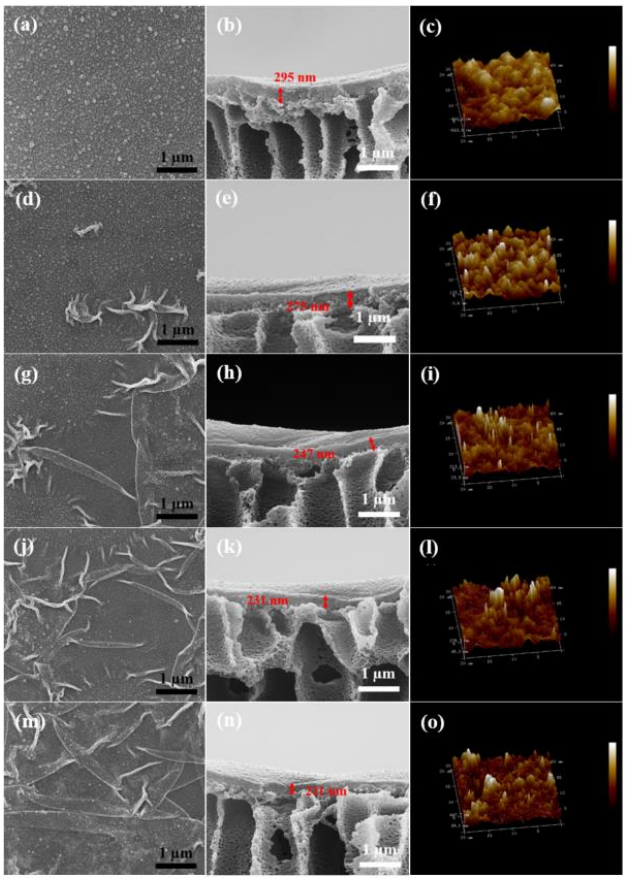

Fig. 4. SEM and AFM characterization of all membranes. Surface SEM images, cross-sectional SEM images, and surface AFM images of all membranes. (a,b,c) PA-0, (d,e,f) PA-0.0025, (g,h,i) PA-0.005, (j,k,l) PA-0.01 and (m,n,o) PA-0.015.

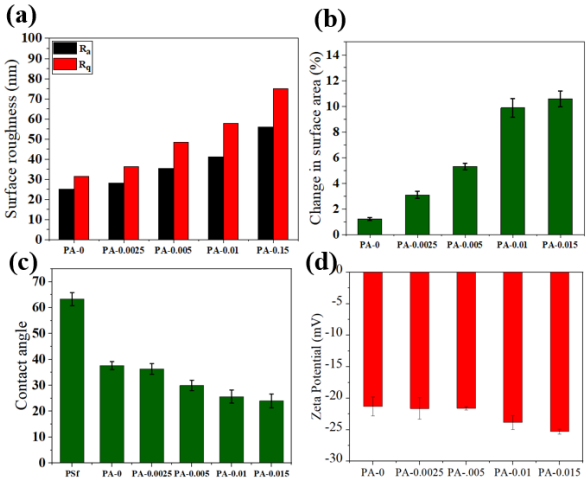

Fig. 5. Membrane characterization: (a) Surface roughness parameters, (b) change in surface area (expressed as the percentage difference in calculated area and projected area), (c) contact angle, and (d) surface zeta potential of all the TFC membrane prepared. Error bars represent the standard deviation of the acquired data.

Apart from this, the surface wettability or the hydrophilicity of a nanofiltration membrane is one of the key characteristics that influence its filtration performance, especially the permeability [45]. Surface wettability is commonly measured by contact angle analysis which is directly associated with the surface functional groups [46]. Therefore, we compared the water contact angle (WCA) of each membrane with PSf support for which the results are presented in Fig. 5c. As anticipated, all NF membranes displayed substantially lower contact angles compared to the PSf membrane support, which was obvious due to the formation of the polyamide layer through interfacial polymerization [47]. Further, the WCA composite PA membranes were lower

than pristine PA-0; which can be attributed to the presence of several hydrophilic functional groups on the underlying NC in the polyamide layer. A reduced contact angle indicates a considerable improvement in the surface hydrophilicity and wettability as compared to pristine membranes, which in turn enhances the membrane permeability. While PSf supports showed a relatively higher WCA of 63.3º, TFC membranes showed an average WCA of 37.7º, 36.3º, 30.1º, 25.67º and 24.1º for PA-0, PA-0.0025, PA-0.005, PA-0.01 and PA-0.015 respectively. The change in WCA between PSf and PA-0 was drastic due to contributions from the surface functional groups formed by interfacial polymerization. However, the incorporation of NC could only improve the hydrophilicity slightly possibly due to the masking effect from the polyamide layer. Although cellulose chains are composed of several hydrophilic functional groups, the presence polyamide layer over the NC could limit its additional contributions. Nevertheless, a noticeable gradual decrease in the WCA was observed upon the increased concentration of NC in the fabrication. Aside from this, the surface zeta potential (Fig. 5d) was also measured to characterize the variations in the surface charge which has a significant impact on the separation performance. The measurements were carried out at a neutral pH similar to the membrane test condition, where membranes displayed zeta potentials between -22 and -25 mV irrespective of their composition [48]. Polyamide membranes are typically characterized by a negative zeta potential arising from the hydrolysis of residual unreacted functional groups of TMC. However, no significant changes in the surface charge were observed due to the presence of NC, possibly due to their low concentration.

3.3. Membrane Performance

The pure water permeance and rejection towards various inorganic salt solutions at 6 bar transmembrane pressure are evaluated to investigate the nanofiltration performance of all synthesized membranes. Firstly, steady-state pure water permeance observed for all the membranes was recorded which is shown in Fig. 6a. As seen in the graph, permeance increased considerably with the addition of NC in the polyamide layer. For instance, while pristine membrane PA-0 offered a permeance of 7.2 ± 0.46 $Lm^{-2}h^{-1}bar^{-1}$, membranes after incorporating NC enhanced to 8.7 ± 0.75 $Lm^{-2}h^{-1}bar^{-1}$, 15.65 ± 1.5 $Lm^{-2}h^{-1}bar^{-1}$, 19.12 ± 1.7 $Lm^{-2}h^{-1}bar^{-1}$ and 25.1 ± 2.2 $Lm^{-2}h^{-1}bar^{-1}$ respectively for PA-0.0025, PA-0.005, PA-0.01 and PA-0.015. Different from some studies in the past that reported a decreased permeance at higher filler loading in the fabrication, we could observe a steady increase in the permeance at all fabrication conditions adopted in this study, thanks to the highly fibrous morphology of NC that prevented pore blocking of the PSf support even at the highest concentration. Accordingly, the highest flux was observed for PA-0.015, which is more than three times of the neat polyamide membrane PA-0. The enhanced water permeability could be attributed to the morphological and surface changes produced by the introduction of NC in the selective layer which will be discussed further in the subsequent sections.

In addition to enhanced permeability, the ability of membranes to maintain their salt rejection is crucial in evaluating their nanofiltration performance. For this, steady state rejection towards 1000 ppm salt solution and corresponding permeance was evaluated for common salts such as NaCl, $MgCl_2$, Na_2SO_4, and $MgSO_4$. When salt solutions were used as a feed, the permeance observed for all membranes was slightly lower than the pure water permeance as shown in Fig. 6b. This decrease in permeance is a typical behavior of nanofiltration membranes and is more pronounced in divalent salt solution due to larger steric hindrance. Therefore, an average decrease of 4.5%, 15.6%, 21%, and 24.8% in the permeance compared to pure water was observed when the salt solution of NaCl, $MgCl_2$, Na_2SO_4, and $MgSO_4$ were respectively used as feed. Our membranes showed remarkably higher rejection towards divalent ions similar to typical TFC-based polyamide membranes. For example, while the rejection of NaCl was below 50% for all cases, the rejection of $MgSO_4$, and Na_2SO_4 stood above 80% for all membranes. It is worth noting that the rejection remained similar for PA-0, PA-0.0025, and PA-0.005 despite a considerable increase in permeance from 7.2 ± 0.46 $Lm^{-2}h^{-1}bar^{-1}$ to 15.65 ± 1.5 $Lm^{-2}h^{-1}bar^{-1}$ indicating that the addition of NC upto 0.005% did not affect the membrane selectivity significantly possibly due to the cross-linking between hydroxyl groups on the cellulose with the TMC [28, 49]. However, upon further increasing the NC, rejection starts to drop and eventually drop below 90% even for $MgSO_4$, and Na_2SO_4 for the case PA-0.015 possibly due to looser polyamide structure and interfacial voids created by a large number of fibers in the cross-linked polymer network [28]. Therefore, considering both permeance and rejection behavior, PA-0.01 could be considered as the optimum membrane exhibiting a pure water permeance of 19.12 ± 1.7 $Lm^{-2}h^{-1}bar^{-1}$ and rejection of 38.1%, 78.1%, 91.6%, and 92.1% respectively towards NaCl, $MgCl_2$, Na_2SO_4, and $MgSO_4$.

The ability of the membrane to sustain its separation performance over a long period of operation is an important parameter considering its potential in practical applications. To examine this, we monitored the long-term performance of PA-0.01 using Na_2SO_4 feed solution over an extended period of time as shown in 6d. With the exception of the initial fluctuation due to compaction, the membrane was able to maintain its permeance and rejection throughout the experiment, demonstrating its capacity for long-term operation. This consistent long-term result supports the potential cross-linking with the TMC that resulted in excellent compatibility of NC in the polymer matrix thereby enhancing the structural integrity of the prepared membranes. Lastly, we compared the performance of PA-01 with some of the recently published TFC membranes modified with cellulose-based materials which are shown in the Fig. 6e. It is apparent that the performance of our membrane is superior to other TFC membranes that utilized various cellulose-based materials such as cellulose nanocrystals [49-52], L-cysteine modified cellulose nanocrystals [53], phosphorylated nano cellulose [54], zwitterionic nano cellulose [55], carboxylated cellulose nanocrystals [56] and sulfated cellulose nanofibril [57] also surpassed the commercial membranes NF270 and NF90 [58].

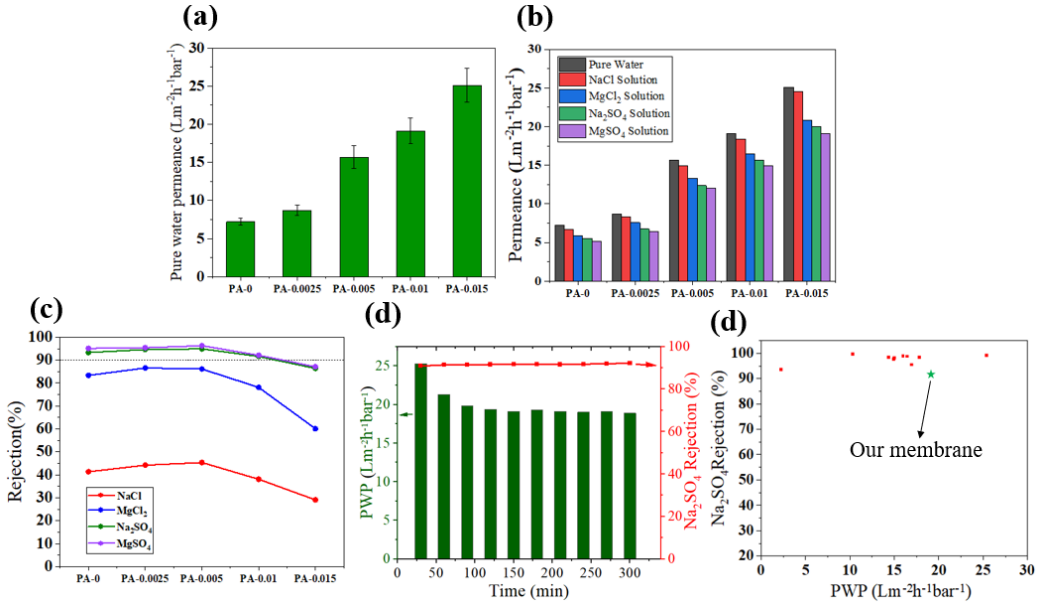

Fig. 6. (a) Pure water permeance (b) salt rejection and (c) salt solution permeance obtained using 1000 ppm for different TFC membranes. (d) Pure water permeance and Na2SO4 rejection during longer filtration time PA-001. (e) Comparison of our membrane performance with other cellulose material-based TFC membranes reported in the literature.

3.4. Role of NC in the membrane performance

The above findings make it evident that the presence of NC has influenced the selective layer properties and eventually affected the overall membrane performance. It is well established that the polyamide formation and subsequently overall membrane performance could be greatly influenced by the variations in membrane support. However, as we employed identical supports for all membrane fabrication, the only difference that may have contributed to the performance improvement would be the variations in the properties of the selective layer. The addition of NC to the aqueous phase resulted in a crumpled morphology of the selective layer as well as an improvement in surface hydrophilicity, which enhanced the permeance compared to pristine TFC membranes. For example, membrane permeance increased by 165% in the case of PA-0.01 compared to PA-0 which strongly emphasizes the role of NC in membrane fabrication. This enhanced performance can be attributed to different changes in the selective layer upon NC incorporation: (1) thinner selective layer (2) crumpled morphology and (3) improved hydrophilicity. Firstly, it is well known that the thinner selective layer offers lower transport resistance leading to faster transport of solvents across the membrane [12, 59, 60]. For example, membrane permeance of ~ 40 $Lm^{-2}h^{-1}bar^{-1}$ was reported for TFC polyamide membranes by fabricating an ultrathin selective layer of ~15 nm [60]. Secondly, morphological variations such as wrinkles or patterns on the selective layer not only provide a more effective filtration area but also introduce interfacial voids [61]. Theoretically, a crumpled morphology can even double the permeance irrespective of the thickness due to the enhancement in the filtration area [62]. Moreover, the presence of interfacial voids in the wrinkles can facilitate additional optimized transport channels minimizing the transport resistance. As commonly understood, a major transport resistance arises in TFC membranes due to the funnel effect caused by the non-porous regions of the membrane support [43, 63]. The funnel effect that limits the deviations from the optimal permeance predicted from a free-standing polyamide layer can be effectively minimized by the presence of big wrinkles covering various pores on the membrane support [43, 63, 64]. As illustrated in the schematic provided in Fig. 7, a smooth TFC membrane with thickness (D)will have several occasions coinciding with non-porous regions of the support with a larger effective transport length (D_{eff}). On the other hand, a crumpled/wrinkled form of the selective layer can effectively bypass these regions due to the presence of interfacial voids. Lastly, the incorporation of amorphous cellulose fibers improved the overall membrane hydrophilicity considerably which is a desired characteristic for enhancing permeability [65].

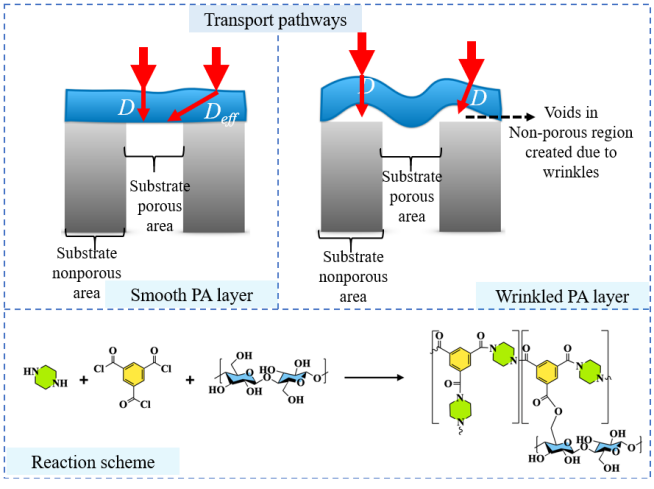

Fig. 7. Top: Illustration of transport pathway in smooth and wrinkled membranes. Bottom: Crosslinking reaction between hydroxyl groups in NC with acyl chloride group of the TMC.

Analyzing the rejection values obtained for different salts, we can see that the incorporation of NC did not bring any significant changes to the separation performance up to a concentration of 0.005%. However, a slight increase in rejection was seen for PA-0.005 compared to PA-0. This marginal increase in rejection could be possibly due to the cross-linking reaction between the hydroxyl functional groups on the cellulose with the acyl chloride groups on the TMC monomers as reported in previous studies [24, 49]. On the other hand, further increasing the NC leads to the deterioration of the selectivity due to interfacial voids. The role of steric hindrance was evident from the results as all membranes generally displayed a higher rejection towards divalent salts [33, 46]. Consequently, rejection towards NaCl was the lowest (< 50%) among the tested salts for all membranes. Furthermore, rejection towards $MgSO_4$ was slightly higher than Na_2SO_4 unlike many of the reported TFC membranes in the past. This can be attributed to the fact that the rejection mechanism is less dependent on the electrostatic repulsion between the charged ions and the membrane surface. If electrostatic repulsion had a significant influence on the separation mechanism, Na_2SO_4 with a low valency cation would experience the highest rejection among the tested ions. In contrast, $MgSO_4$ made up of larger hydrated divalent ions showed the highest rejection implying steric hindrance as the dominating mechanism of rejection [66, 67]. It is worth highlighting that, although the flux of the membrane increased substantially, only a negligible contribution towards an enhancement in the rejection behavior of the membranes was realized upon NC incorporation. Thus, we can reasonably conclude that the addition of NC has a significant impact on the permeance than the selectivity of the composite membranes.

4. Conclusion

In summary, low-cost, sustainable, and environmentally friendly NC with highly networked structures has been successfully incorporated into the polyamide layer of the TFC NF membrane during interfacial polymerization. The NC/TFC membranes showed greatly enhanced permeability with the integration of NC in the aqueous phase during membrane fabrication. At a loading of 0.001 wt% NC in the amine solution, the membrane permeance increased to 19.12 ± 1.7 $Lm^{-2}h^{-1}bar^{-1}$ which is more than 165% compared to the neat TFC membrane, whilst rejection towards divalent salts remained above 90%. The improved performance could be attributed to the changes in the polyamide layer due to the presence of NC during interfacial polymerization. Considering that NC is derived from sustainable and renewable resources, the enhanced membrane performance is promising for seawater desalination and other water treatment applications.

Acknowledgments

This work was supported by the New York University Abu Dhabi (NYUAD) Water Research Center and funded by the Tamkeen Research Institute Award (project CG007). The authors would like to acknowledge James Weston (AFM) and Core Technology Platform for assisting with this work.

Data availability

Data will be available upon request.

Funding

This research did not receive any specific grant from funding agencies in the public, commercial, or not-for-profit sectors.

Declaration of Competing Interest

The authors declare that they have no known competing financial interests or personal relationships that could have appeared to influence the work reported in this paper.

CRediT authorship contribution statement

S. Mohammed: Conceptualization, Methodology, Investigation, Data curation, Investigation, Writing - original draft.
J. Aburabie: Investigation.
R. Hashaikeh: Funding acquisition, Supervision, Writing – review & editing

References

[1] A. Boretti and L. Rosa, "Reassessing the projections of the world water development report," NPJ Clean Water, vol. 2, no. 1, p. 15, 2019, doi: https://doi.org/10.1038/s41545-019-0039-9.
[2] P. Chowdhary, R. N. Bharagava, S. Mishra, and N. Khan, "Role of industries in water scarcity and its adverse effects on environment and human health," Environmental Concerns and Sustainable Development:

Volume 1: Air, Water and Energy Resources, pp. 235-256, 2020, doi: https://doi.org/10.1007/978-981-13-5889-0.
[3] M. Issaoui, S. Jellali, A. A. Zorpas, and P. Dutournie, "Membrane technology for sustainable water resources management: Challenges and future projections," Sustainable Chemistry and Pharmacy, vol. 25, p. 100590, 2022/04/01/ 2022, doi: https://doi.org/10.1016/j.scp.2021.100590.
[4] D. L. Oatley-Radcliffe, M. Walters, T. J. Ainscough, P. M. Williams, A. W. Mohammad, and N. Hilal, "Nanofiltration membranes and processes: A review of research trends over the past decade," Journal of Water Process Engineering, vol. 19, pp. 164-171, 2017, doi: https://doi.org/10.1016/j.jwpe.2017.07.026.
[5] A. Khalil, S. Mohammed, R. Hashaikeh, and N. Hilal, "Lithium recovery from brine: Recent developments and challenges," Desalination, vol. 528, p. 115611, 2022, doi: https://doi.org/10.1016/j.desal.2022.115611.
[6] N. G. Domenech, F. Purcell-Milton, and Y. K. Gun'ko, "Recent progress and future prospects in the development of advanced materials for nanofiltration," Materials Today Communications, vol. 23, p. 100888, 2020, doi: https://doi.org/10.1016/j.mtcomm.2019.100888.
[7] S. Mohammed, "Graphene oxide: A mini-review on the versatility and challenges as a membrane material for solvent-based separation," Chemical Engineering Journal Advances, p. 100392, 2022, doi: https://doi.org/10.1016/j.ceja.2022.100392.
[8] S. Tul Muntha, A. Kausar, and M. Siddiq, "Advances in polymeric nanofiltration membrane: A review," Polymer-Plastics Technology and Engineering, vol. 56, no. 8, pp. 841-856, 2017, doi: https://doi.org/10.1080/03602559.2016.1233562.
[9] V. V. Bhaskar and N. J. Kaleekkal, "Next-generation thin-film composite nanofiltration membranes for water remediation: A review," Emergent Materials, pp. 1-18, 2021, doi: https://doi.org/10.1007/s42247-021-00273-8.
[10] W. Lau, S. Gray, T. Matsuura, D. Emadzadeh, J. P. Chen, and A. Ismail, "A review on polyamide thin film nanocomposite (TFN) membranes: History, applications, challenges and approaches," Water Research, vol. 80, pp. 306-324, 2015. doi: https://doi.org/10.1016/j.watres.2015.04.037.
[11] G.-Y. Chai and W. B. Krantz, "Formation and characterization of polyamide membranes via interfacial polymerization," Journal of Membrane Science, vol. 93, no. 2, pp. 175-192, 1994, doi: https://doi.org/10.1016/0376-7388(94)80006-5.
[12] S. Karan, Z. Jiang, and A. G. Livingston, "Sub–10 nm polyamide nanofilms with ultrafast solvent transport for molecular separation," Science, vol. 348, no. 6241, pp. 1347-1351, 2015, doi: https://doi.org/10.1126/science.aaa5058.
[13] Z. Liao, J. Zhu, X. Li, and B. Van der Bruggen, "Regulating composition and structure of nanofillers in thin film nanocomposite (TFN) membranes for enhanced separation performance: A critical review," Separation and Purification Technology, vol. 266, p. 118567, 2021/07/01/ 2021, doi: https://doi.org/10.1016/j.seppur.2021.118567.
[14] N. Akther, S. Phuntsho, Y. Chen, N. Ghaffour, and H. K. Shon, "Recent advances in nanomaterial-modified polyamide thin-film composite membranes for forward osmosis processes," Journal of Membrane Science, vol. 584, pp. 20-45, 2019/08/15/ 2019, doi: https://doi.org/10.1016/j.memsci.2019.04.064.
[15] N. Zhang, X. Song, H. Jiang, and C. Y. Tang, "Advanced thin-film nanocomposite membranes embedded with organic-based nanomaterials for water and organic solvent purification: A review," Separation and Purification Technology, vol. 269, p. 118719, 2021/08/15/ 2021, doi: https://doi.org/10.1016/j.seppur.2021.118719.
[16] X. Wei, Y. Liu, J. Zheng, X. Wang, S. Xia, and B. Van der Bruggen, "A critical review on thin-film nanocomposite membranes enabled by nanomaterials incorporated in different positions and with diverse dimensions: Performance comparison and mechanisms," Journal of Membrane Science, vol. 661, p. 120952, 2022/11/05/ 2022, doi: https://doi.org/10.1016/j.memsci.2022.120952.
[17] X. Zhang, C. Liu, J. Yang, C.-Y. Zhu, L. Zhang, and Z.-K. Xu, "Nanofiltration membranes with hydrophobic microfiltration substrates for robust structure stability and high water permeation flux," Journal of Membrane Science, vol. 593, p. 117444, 2020, doi: https://doi.org/10.1016/j.memsci.2019.117444.
[18] A. K. Rana, V. K. Gupta, A. K. Saini, S. I. Voicu, M. H. Abdellattifaand, and V. K. Thakur, "Water desalination using nanocelluloses/cellulose derivatives based membranes for sustainable future," Desalination, vol. 520, p. 115359, 2021, doi: https://doi.org/10.1016/j.desal.2021.115359.
[19] S. Muhmed et al., "Emerging chitosan and cellulose green materials for ion exchange membrane fuel cell: a review," Energy, Ecology and Environment, vol. 5, pp. 85-107, 2020, doi: https://doi.org/10.1007/S40974-019-00127-4.
[20] S. Liu, Z. X. Low, Z. Xie, and H. Wang, "TEMPO-Oxidized Cellulose Nanofibers: A Renewable Nanomaterial for Environmental and Energy Applications," Advanced Materials Technologies, vol. 6, no. 7, p. 2001180, 2021, doi: https://doi.org/10.1002/admt.202001180.
[21] A. J. Sayyed, D. V. Pinjari, S. H. Sonawane, B. A. Bhanvase, J. Sheikh, and M. Sillanpää, "Cellulose-based nanomaterials for water and wastewater treatments: A review," Journal of Environmental Chemical Engineering, vol. 9, no. 6, p. 106626, 2021, doi: https://doi.org/10.1016/j.jece.2021.106626.
[22] Y. Ying et al., "Recent advances of nanomaterial-based membrane for water purification," Applied Materials Today, vol. 7, pp. 144-158, 2017, doi: https://doi.org/10.1016/j.apmt.2017.02.010.
[23] R. Hashaikeh and H. Abushammala, "Acid mediated networked cellulose: Preparation and characterization," Carbohydrate polymers, vol. 83, no. 3, pp. 1088-1094, 2011, doi: https://doi.org/10.1016/j.carbpol.2010.08.081.
[24] S. Liu et al., "Robust hilly polyamide membrane for fast desalination," ACS Applied Polymer Materials, vol. 3, no. 2, pp. 1070-1077, 2021, doi: https://doi.org/10.1021/acsapm.0c01230.
[25] F. Soyekwo et al., "Cellulose nanofiber intermediary to fabricate highly-permeable ultrathin nanofiltration membranes for fast water purification," Journal of Membrane Science, vol. 524, pp. 174-185, 2017/02/15/ 2017, doi: https://doi.org/10.1016/j.memsci.2016.11.019.
[26] J. Kong, Y. Zhu, D. Dong, and J. Jin, "Ultrapermeable polyamide nanofiltration membrane formed on a self-constructed cellulose nanofibers interlayer," Chemical Engineering Research and Design, vol. 179, pp. 249-256, 2022/03/01/ 2022, doi: https://doi.org/10.1016/j.cherd.2022.01.032.
[27] J. L. Fajardo-Diaz et al., "Low-pressure reverse osmosis membrane made of cellulose nanofiber and carbon nanotube polyamide nano-nanocomposite for high purity water production," Chemical Engineering Journal, vol. 448, p. 137359, 2022/11/15/ 2022, doi: https://doi.org/10.1016/j.cej.2022.137359.
[28] S. Liu et al., "Enhancement of desalination performance of thin-film nanocomposite membrane by cellulose nanofibers," Journal of Membrane Science, vol. 592, p. 117363, 2019/12/15/ 2019, doi: https://doi.org/10.1016/j.memsci.2019.117363.
[29] Z. Wang et al., "Nanoparticle-templated nanofiltration membranes for ultrahigh performance desalination," Nature Communications, vol. 9, no. 1, p. 2004, 2018, doi: https://doi.org/10.1038/s41467-018-04467-3.
[30] J. Aburabie, A. Eskhan, and R. Hashaikeh, "Shifting to Transparent/Hazy Properties: The Case of Alginate/Network Cellulose All-Polysaccharide Composite Films," Macromolecular Rapid Communications, vol. 43, no. 17, p. 2200172, 2022, doi: https://doi.org/10.1002/marc.202200172.
[31] S. Mohammed, J. Aburabie, H. Nassrullah, and R. Hashaikeh, "Porous rGO/networked cellulose composite membranes: Towards enhanced nanofiltration performance of rGO-based membranes," Materials Today Sustainability, vol. 25, p. 100682, 2024/03/01/ 2024, doi: https://doi.org/10.1016/j.mtsust.2024.100682.
[32] S. Mohammed, H. Nassrullah, J. Aburabie, and R. Hashaikeh, "Fabrication of Thin Film Composite Membranes on Nanozeolite Modified Support Layer for Tailored Nanofiltration Performance," Membranes, vol. 12, no. 10, p. 940, 2022, doi: https://doi.org/10.3390/membranes12100940.
[33] S. Mohammed, H. M. Hegab, and R. Ou, "Nanofiltration performance of glutaraldehyde crosslinked graphene oxide-cellulose nanofiber membrane," Chemical Engineering Research and Design, vol. 183, pp. 1-12, 2022, doi: https://doi.org/10.1016/j.cherd.2022.04.039.
[34] J. Aburabie, S. Mohammed, H. Nassrullah, and R. Hashaikeh, "Electrically-conductive, Joule-heated pervaporation membranes for desalination: Investigating energy-saving, self-cleaning and anti-swelling trifecta," Desalination, vol. 564, p. 116769, 2023/10/15/ 2023, doi: https://doi.org/10.1016/j.desal.2023.116769.
[35] J. Aburabie, B. Lalia, and R. Hashaikeh, "Proton conductive, low methanol crossover cellulose-based membranes," Membranes, vol. 11, no. 7, p. 539, 2021, doi: https://doi.org/10.3390/membranes11070539.
[36] W. H. Wan Ishak, N. A. Rosli, and I. Ahmad, "Influence of amorphous cellulose on mechanical, thermal, and hydrolytic degradation of poly (lactic acid) biocomposites," Scientific Reports, vol. 10, no. 1, p. 11342, 2020, doi: https://doi.org/10.1038%2Fs41598-020-68274-x.
[37] L. Shen, W.-s. Hung, J. Zuo, X. Zhang, J.-Y. Lai, and Y. Wang, "High-performance thin-film composite polyamide membranes developed with green ultrasound-assisted interfacial polymerization," Journal of membrane science, vol. 570, pp. 112-119, 2019, doi: https://doi.org/10.1016/j.memsci.2018.10.014.
[38] S. Mohammed, J. Aburabie, and R. Hashaikeh, "Facile morphological tuning of thin film composite membranes for enhanced desalination performance," npj Clean Water, vol. 6, no. 1, p. 55, 2023, doi: https://doi.org/10.1038/s41545-023-00271-9.

[39] P. P. Sharma, S. Mohammed, J. Aburabie, and R. Hashaikeh, "Valorization of Seawater Reverse Osmosis Brine by Monovalent Ion-Selective Membranes through Electrodialysis," Membranes, vol. 13, no. 6, p. 562, 2023, doi: https://doi.org/10.3390/membranes13060562.

[40] D. Hu, X. Ren, H. Fu, Y. Wang, X. Feng, and H. Li, "Constructing highly rough skin layer of thin film (nano) composite polyamide membranes to enhance separation performance: A review," Journal of Applied Polymer Science, vol. 139, no. 30, p. e52692, 2022, doi: https://doi.org/10.1002/app.52692.

[41] Z. Zhang, X. Shi, R. Wang, A. Xiao, and Y. Wang, "Ultra-permeable polyamide membranes harvested by covalent organic framework nanofiber scaffolds: a two-in-one strategy," Chemical Science, 10.1039/C9SC03088C vol. 10, no. 39, pp. 9077-9083, 2019, doi: https://doi.org/10.1039/C9SC03088C.

[42] S. Han, Z. Wang, S. Cong, J. Zhu, X. Zhang, and Y. Zhang, "Root-like polyamide membranes with fast water transport for high-performance nanofiltration," Journal of Materials Chemistry A, vol. 8, no. 47, pp. 25028-25034, 2020, doi: https://doi.org/10.1039/D0TA06520J.

[43] L. E. Peng, Z. Yang, L. Long, S. Zhou, H. Guo, and C. Y. Tang, "A critical review on porous substrates of TFC polyamide membranes: Mechanisms, membrane performances, and future perspectives," Journal of Membrane Science, vol. 641, p. 119871, 2022/01/01/ 2022, doi: https://doi.org/10.1016/j.memsci.2021.119871.

[44] Y. Hao et al., "An ultrahighly permeable-selective nanofiltration membrane mediated by an in situ formed interlayer," Journal of Materials Chemistry A, vol. 8, no. 10, pp. 5275-5283, 2020, doi: https://doi.org/10.1039/C9TA12258C.

[45] L. Francis, S. Mohammed, R. Hashaikeh, and N. Hilal, "Fabrication and characterization of superhydrophilic graphene-based electrospun membranes for efficient oil-water separation," Journal of Water Process Engineering, vol. 54, p. 104066, 2023, doi: https://doi.org/10.1016/j.jwpe.2023.104066.

[46] S. Mohammed et al., "Effect of oxygen plasma treatment on the nanofiltration performance of reduced graphene oxide/cellulose nanofiber composite membranes," Green Chemical Engineering, vol. 2, no. 1, pp. 122-131, 2021, doi: https://doi.org/10.1016/j.gce.2020.12.001.

[47] M. B. M. Y. Ang et al., "Improved performance of thin-film nanofiltration membranes fabricated with the intervention of surfactants having different structures for water treatment," Desalination, vol. 481, p. 114352, 2020/05/01/ 2020, doi: https://doi.org/10.1016/j.desal.2020.114352.

[48] F. Baskoro et al., "Graphene oxide-cation interaction: Inter-layer spacing and zeta potential changes in response to various salt solutions," Journal of Membrane Science, vol. 554, pp. 253-263, 2018/05/15/ 2018, doi: https://doi.org/10.1016/j.memsci.2018.03.006.

[49] L. Bai et al., "Incorporation of Cellulose Nanocrystals (CNCs) into the Polyamide Layer of Thin-Film Composite (TFC) Nanofiltration Membranes for Enhanced Separation Performance and Antifouling Properties," Environmental Science & Technology, vol. 52, no. 19, pp. 11178-11187, 2018/10/02 2018, doi: http://dx.doi.org/10.1021/acs.est.8b04102.

[50] S. Huang et al., "Polyamide nanofiltration membranes incorporated with cellulose nanocrystals for enhanced water flux and chlorine resistance," ACS Sustainable Chemistry & Engineering, vol. 7, no. 14, pp. 12315-12322, 2019, doi: https://doi.org/10.1021/acssuschemeng.9b01651.

[51] L. Bai, Y. Liu, A. Ding, N. Ren, G. Li, and H. Liang, "Fabrication and characterization of thin-film composite (TFC) nanofiltration membranes incorporated with cellulose nanocrystals (CNCs) for enhanced desalination performance and dye removal," Chemical Engineering Journal, vol. 358, pp. 1519-1528, 2019, doi: https://doi.org/10.1016/j.cej.2018.10.147.

[52] Y. Rahimi-Kashkouli, M. Rahbari-Sisakht, and A. G. J. Ghadam, "Thin film nanocomposite nanofiltration membrane incorporated with cellulose nanocrystals with superior anti-organic fouling affinity," Environmental Science: Water Research & Technology, vol. 6, no. 3, pp. 715-723, 2020, doi: https://doi.org/10.1039/C9EW00963A.

[53] F. Abedi, M. A. Dubé, D. Emadzadeh, and B. Kruczek, "Improving nanofiltration performance using modified cellulose nanocrystal-based TFN membranes," Journal of Membrane Science, vol. 670, p. 121369, 2023/03/15/ 2023, doi: https://doi.org/10.1016/j.memsci.2023.121369.

[54] Z. Wang, D. Xia, B. Wang, H. Liu, and L. Zhu, "Highly permeable polyamide nanofiltration membrane incorporated with phosphorylated nanocellulose for enhanced desalination," Journal of Membrane Science, vol. 647, p. 120339, 2022/04/05/ 2022, doi: https://doi.org/10.1016/j.memsci.2022.120339.

[55] D. Xia, M. Zhang, C. Tong, Z. Wang, H. Liu, and L. Zhu, "In-situ incorporating zwitterionic nanocellulose into polyamide nanofiltration membrane towards excellent perm-selectivity and antifouling performances," Desalination, vol. 521, p. 115397, 2022, doi: https://doi.org/10.1016/j.desal.2021.115397.

[56] Y. Liu et al., "The role of carboxylated cellulose nanocrystals placement in the performance of thin-film composite (TFC) membrane," Journal of Membrane Science, vol. 617, p. 118581, 2021, doi: https://doi.org/10.1016/j.memsci.2020.118581.

[57] W. Li, X. Wang, M. He, Z. Zhang, J. Chen, and G. Yang, "Fabrication of high-performance nanofiltration membranes by using sulfated cellulose nanofibril as the intermediate support layer," Desalination, vol. 532, p. 115741, 2022, doi: https://doi.org/10.1016/j.desal.2022.115741.

[58] K. Boussu et al., "Characterization of polymeric nanofiltration membranes for systematic analysis of membrane performance," Journal of Membrane Science, vol. 278, no. 1-2, pp. 418-427, 2006, doi: https://doi.org/10.1016/j.memsci.2005.11.027.

[59] C.-Y. Zhu, C. Liu, J. Yang, B.-B. Guo, H.-N. Li, and Z.-K. Xu, "Polyamide nanofilms with linearly-tunable thickness for high-performance nanofiltration," Journal of Membrane Science, vol. 627, p. 119142, 2021/06/01/ 2021, doi: https://doi.org/10.1016/j.memsci.2021.119142.

[60] S. Gao, Y. Zhu, Y. Gong, Z. Wang, W. Fang, and J. Jin, "Ultrathin Polyamide Nanofiltration Membrane Fabricated on Brush-Painted Single-Walled Carbon Nanotube Network Support for Ion Sieving," ACS Nano, vol. 13, no. 5, pp. 5278-5290, 2019/05/28 2019, doi: https://doi.org/10.1021/acsnano.8b09761.

[61] F. Gao et al., "Polyamide membrane with nanoscale stripes and internal voids for high-performance nanofiltration," Journal of Membrane Science, vol. 671, p. 121406, 2023/04/05/ 2023, doi: https://doi.org/10.1016/j.memsci.2023.121406.

[62] S. Shao et al., "Nanofiltration Membranes with Crumpled Polyamide Films: A Critical Review on Mechanisms, Performances, and Environmental Applications," Environmental Science & Technology, vol. 56, no. 18, pp. 12811-12827, 2022/09/20 2022, doi: https://doi.org/10.1021/acs.est.2c04736.

[63] F. Wang, Z. Yang, and C. Y. Tang, "Modeling water transport in interlayered thin-film nanocomposite membranes: gutter effect vs funnel effect," ACS ES&T Engineering, vol. 2, no. 11, pp. 2023-2033, 2022, doi: https://doi.org/10.1021/acsestengg.2c00133.

[64] L. Long, C. Wu, Z. Yang, and C. Y. Tang, "Carbon nanotube interlayer enhances water permeance and antifouling performance of nanofiltration membranes: mechanisms and experimental evidence," Environmental Science & Technology, vol. 56, no. 4, pp. 2656-2664, 2022, doi: https://doi.org/10.1021/acs.est.1c07332.

[65] M. Mänttäri, A. Pihlajamäki, and M. Nyström, "Effect of pH on hydrophilicity and charge and their effect on the filtration efficiency of NF membranes at different pH," Journal of Membrane Science, vol. 280, no. 1-2, pp. 311-320, 2006, doi: https://doi.org/10.1016/j.memsci.2006.01.034.

[66] J. Schaep, B. Van der Bruggen, C. Vandecasteele, and D. Wilms, "Influence of ion size and charge in nanofiltration," Separation and Purification Technology, vol. 14, no. 1-3, pp. 155-162, 1998, doi: https://doi.org/10.1016/S1383-5866(98)00070-7.

[67] B. Tansel et al., "Significance of hydrated radius and hydration shells on ionic permeability during nanofiltration in dead-end and cross-flow modes," Separation and Purification Technology, vol. 51, no. 1, pp. 40-47, 2006/08/01/ 2006, doi: https://doi.org/10.1016/j.seppur.2005.12.020.

SUPPLEMENTARY INFORMATION

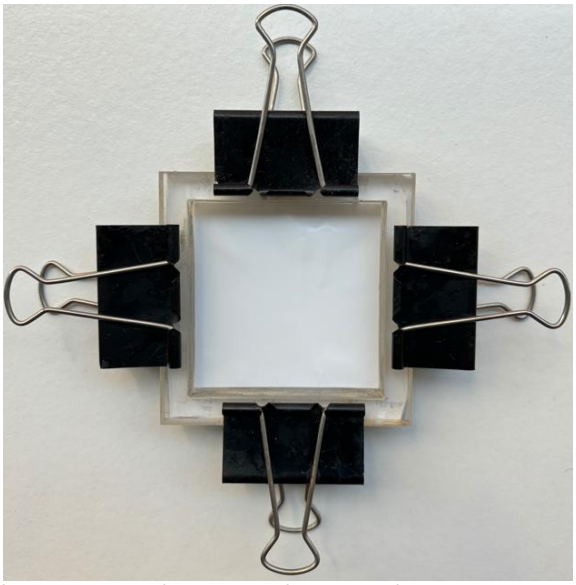

Figure S8: Plate and frame assembly specifically designed for membrane fabrication through interfacial polymerization.

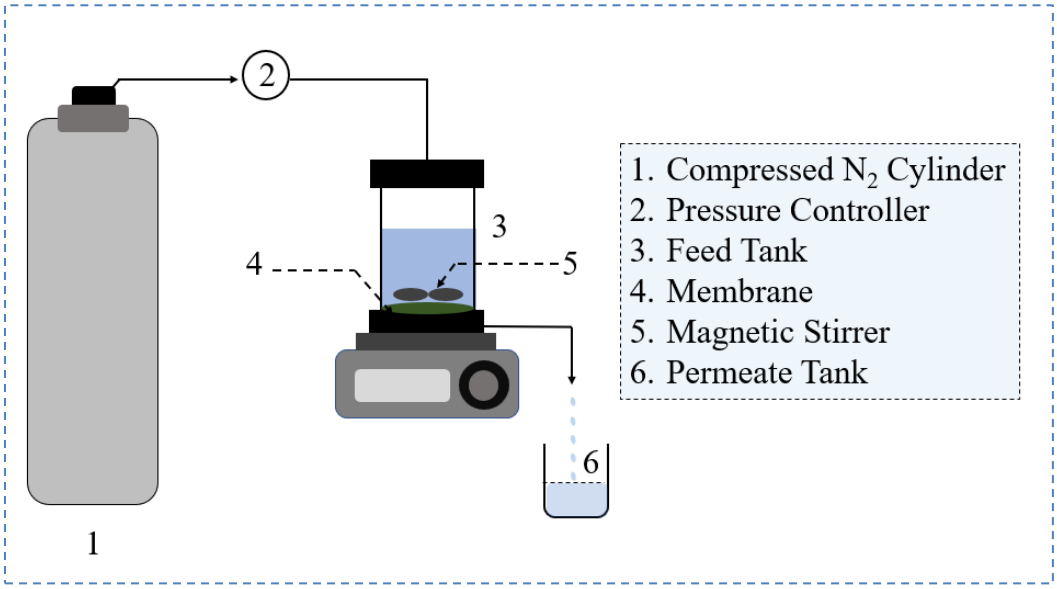

Figure S9: A schematic representation of a dead-end filtration system that is used to assess the nanofiltration performance of PA membranes.

Figure S10: NC dispersion in water.

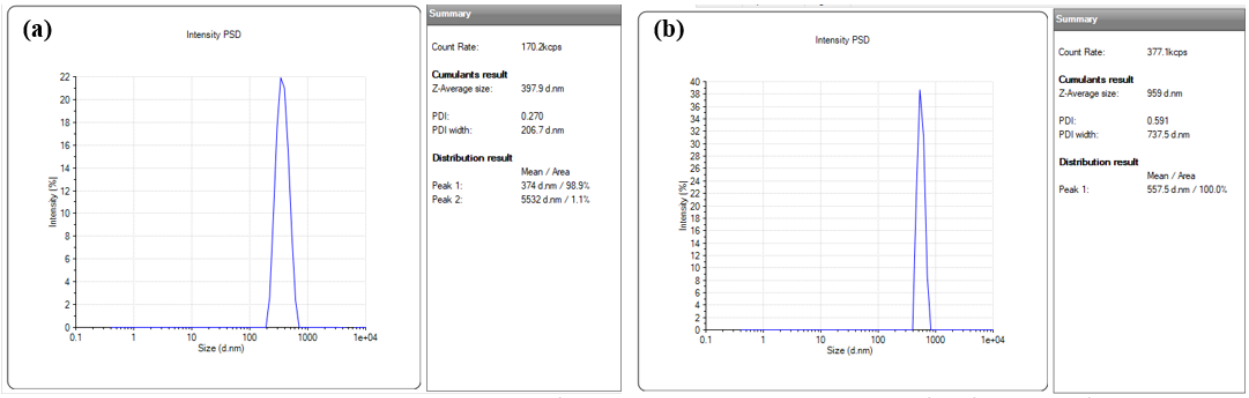

Figure S11: DLS measurement on 0.01% of the (a) initial NC solution and (b) NC solution after refining by centrifuge.